

Electronic energy-level structure, correlation crystal-field effects, and f - f transition intensities of Er^{3+} in $\text{Cs}_3\text{Lu}_2\text{Cl}_9$

Stefan R. Lüthi and Hans U. Güdel*

Departement für Chemie und Biochemie, Universität Bern, Freiestrasse 3, CH-3000 Bern 9, Switzerland

Markus P. Hehlen

Optical Sciences Laboratory, The University of Michigan, 1301 Beal Avenue, Ann Arbor, Michigan 48109-2122

John R. Quagliano

Chemical Science and Technology Division, Los Alamos National Laboratory, Mail stop E543, Los Alamos, New Mexico 87545

(Received 16 January 1998)

Single crystals of 1% Er^{3+} -doped $\text{Cs}_3\text{Lu}_2\text{Cl}_9$ were grown using the Bridgman technique. From highly resolved polarized absorption spectra measured at 10 and 16 K, and upconversion luminescence and excitation spectra measured at 4.2 K, 114 crystal-field levels from $27\ ^{2S+1}L_J(4f^{11})$ multiplets of Er^{3+} were assigned. 111 of these were used for a semiempirical computational analysis. A Hamiltonian including only electrostatic, spin-orbit, and one-particle crystal-field interactions (C_{3v}) yielded a root-mean-square standard deviation of $159.8\ \text{cm}^{-1}$ and could not adequately reproduce the experimental crystal-field energies. The additional inclusion of two- and three-body atomic interactions, giving a Hamiltonian with 16 atomic and 6 crystal-field parameters, greatly reduced the rms standard deviation to $22.75\ \text{cm}^{-1}$. The further inclusion of the correlation crystal-field interaction \hat{g}_{10A}^4 again lowered the rms standard deviation to a final value of $17.98\ \text{cm}^{-1}$ and provided substantial improvement in the calculated crystal-field splittings of mainly the $J=9/2$ or $J=11/2$ multiplets. However, the calculated baricenter energies of some excited-state multiplets deviate from their respective experimental values, and improvements in the atomic part of the effective Hamiltonian are required to correct this deficiency of the model. On the basis of the calculated electronic wave functions, the 12 electric-dipole intensity parameters (C_{3v}) of the total transition dipole strength were obtained from a fit to 95 experimental crystal-field transition intensities. The overall agreement between experimental and calculated intensities is fair. The discrepancies are most likely a result of using the approximate C_{3v} rather than the actual C_3 point symmetry of Er^{3+} in $\text{Cs}_3\text{Lu}_2\text{Cl}_9$ in the calculations. [S0163-1829(98)02024-4]

I. INTRODUCTION

Among the trivalent lanthanides Er^{3+} has a particularly favorable electronic energy-level structure for energy upconversion processes. Luminescence in the visible (VIS) spectral range upon near-infrared (NIR) excitation is thus very common in most Er^{3+} compounds, and the underlying upconversion processes have been studied extensively.¹⁻³ Upconversion laser action around 470, 550, and 670 nm has been reported for Er^{3+} -doped heavy-metal fluorozirconate glass fibers,^{4,5} and for Er^{3+} -doped crystals of BaY_2F_8 ,^{6,7} YAlO_3 ,⁸ BaYb_2F_8 ,⁹ and YLiF_4 ,¹⁰⁻¹⁴ upon pumping around 800, 840, 980, and 1045 nm with a Ti:sapphire or semiconductor diode laser.

Two principal upconversion mechanisms are operative: (i) excited-state absorption (ESA) on a single Er^{3+} ion and (ii) energy-transfer upconversion (ETU) involving two or more excited Er^{3+} ions in close proximity. The efficiency of both these processes, but of the ESA process in particular, critically depends on the energy match of the involved excitation steps.¹⁵ The optimization of upconversion processes in Er^{3+} compounds, so far, has been largely based on trial and error. Compared to oxide-based materials, low-energy phonon materials such as halide crystals and glasses generally have strongly enhanced luminescence quantum yields for NIR-to-

VIS upconversion. But even there, the actual efficiencies of the various upconversion processes are largely determined by details in the electronic and vibrational properties of the material. A recent study on Er^{3+} -doped LaCl_3 (Ref. 16) demonstrated that the quantitative prediction of the upconversion behavior of an Er^{3+} compound, considered impossible up to now, is actually feasible. A detailed knowledge of all the crystal-field states up to about $30\ 000\ \text{cm}^{-1}$ and of the oscillator strengths of all the electronic transitions between them is a prerequisite for such a prediction. Part of this knowledge can be gained from high-resolution absorption spectroscopy, but the intensities of the very important transitions between excited states are not easily accessible. This key information can be obtained from a calculation based on extensive absorption data.

The often employed Judd-Ofelt analysis only provides a rough approximation to transition intensities. Although being straightforward and yielding useful results, the Judd-Ofelt model is restricted to multiplet-to-multiplet transitions since crystal-field splittings are neglected.^{17,18} Potential multiplet-to-multiplet laser transitions can thus be identified,^{19,20} but a much finer understanding is required for the quantitative prediction of upconversion mechanisms or the identification of potential laser transitions. Crystal-field effects have to be taken into account, and crystal-field splittings should be predictable to within 10 – $20\ \text{cm}^{-1}$. Reid, Richardson, and their

co-workers developed models that take into account a variety of interactions, and energy-level calculations for the entire lanthanide series in the cubic elpasolite host material $\text{Cs}_2\text{NaYCl}_6$ (Ref. 21) have been reported.

Recent studies on Er^{3+} -doped CsCdBr_3 (Ref. 22) and $\text{Cs}_3\text{Lu}_2\text{Br}_9$,²³ in which Er^{3+} occupies a trigonal site such as in the title compound, have established the importance of correlation crystal-field (CCF) terms in the effective Hamiltonian for obtaining a satisfactory reproduction of energies and intensities. The results of these latter studies served as a starting point for the present work. Our experimental data set is unusually extensive, and besides the energies and intensities of the transitions we have the irreducible representations (irrep) of the crystal-field states from the clear-cut polarization properties of the absorption and emission lines. In Secs. V A–V C we determine and refine a parameter set that best reproduces the 114 observed crystal-field energies and the polarization properties between 0 and $43\,450\text{ cm}^{-1}$. The wave functions thus obtained are used in Sec. V D to compute crystal-field transition intensities. We show that the energies can be predicted to within the targeted $10\text{--}20\text{ cm}^{-1}$ using a detailed 23 parameter Hamiltonian. The accuracy of the respective wave functions, however, proves not to be high enough for a satisfactory description of crystal-field transition intensities, the reason being the approximate point symmetry of the Hamiltonian.

II. EXPERIMENT

A. Sample preparation

Analogous to other $\text{Cs}_3\text{M}_2\text{Cl}_9$ (where M =lanthanide), $\text{Cs}_3\text{Lu}_2\text{Cl}_9$ represents an incongruently melting phase,²⁴ which forms from the reaction of CsCl and LuCl_3 . The starting materials as well as $\text{Cs}_3\text{Lu}_2\text{Cl}_9:1\% \text{Er}^{3+}$ are highly hygroscopic, requiring crystal growth and sample preparation to be carried out in a dry ($<0.1\text{ ppm H}_2\text{O}$) inert atmosphere. Dry powders of CsCl , LuCl_3 , and ErCl_3 were prepared, and sublimed for purification as described in Ref. 25. From these binary halides single crystals of $\text{Cs}_3\text{Lu}_2\text{Cl}_9:1\% \text{Er}^{3+}$ were grown in silica ampoules using the Bridgman technique. The optical orientation of the single crystals and the determination of the c axis was achieved using a microscope with crossed polarizers. From a single crystal sealed in resin (Buehler Castrolite), a plate parallel to the main crystal axis (c) was cut with a diamond saw. The plate was polished to optical quality with dry Al_2O_3 powders of decreasing particle size down to $0.3\ \mu\text{m}$ in dry paraffin oil. The sample was then mounted in a copper cell with silica windows for the spectroscopic measurements.

B. Spectroscopic experiments

Absorption spectra with the electric vector of the light polarized parallel ($E\parallel c$, π spectrum) and perpendicular ($E\perp c$, σ spectrum) to the unique axis were recorded in the range $1600\text{--}220\text{ nm}$ on a Cary 5E spectrometer (Varian). Spectral bandwidths of 0.18 cm^{-1} in the NIR, 0.4 cm^{-1} in the VIS, and 0.8 cm^{-1} in the near-ultraviolet (UV) region were achieved.

Polarized upconversion luminescence and excitation spectra were performed using an argon-ion laser (Spectra Physics

2045) pumped Ti:sapphire laser (Schwartz Electrooptics). The sample luminescence was dispersed by a 0.85-m double monochromator (Spex 1402) using 500 nm blazed 1200 grooves/mm gratings and detected by a cooled photomultiplier (RCA 31034) using a photon counting system (Stanford Research SR400). The spectral resolution for the upconversion luminescence and excitation spectra was typically 1.0 and 1.5 cm^{-1} , respectively.

A closed-cycle helium cryostat (Air Products Displex) was used for sample cooling to 10 K in the absorption measurements. For the upconversion luminescence and excitation experiments the sample was immersed in liquid helium at 4.2 K in a bath cryostat (Oxford Instruments MD4).

III. MODEL OF THE $4f^{11}$ ELECTRONIC ENERGY-LEVEL STRUCTURE

A. Crystal-field energy calculation

The $[\text{Xe}]4f^{11}$ electron configuration of Er^{3+} gives rise to a total of $41\ 2^{2S+1}L_J$ multiplets. The crystal-field symmetry at the Er^{3+} site in $\text{Cs}_3\text{Lu}_2\text{Cl}_9$ is approximately C_{3v} (see Sec. V A) and consequently splits each of the multiplets into $(2J+1)/2$ Kramers doublets, resulting in 182 doubly degenerate $2^{2S+1}L_J(M_J)$ crystal-field states. The individual energies of these crystal-field states are obtained from the diagonalization of the full $|SLJM_J\rangle$ matrix of a semiempirical effective Hamiltonian \hat{H} . In contrast to the angular part of \hat{H} , which can be solved analytically, the radial part of the various interactions has to be parametrized. The parameter values are obtained from a least-squares fitting procedure of \hat{H} to a set of experimental electronic energy levels. The Hamiltonian is defined as

$$\hat{H} = \hat{H}_a + \hat{H}_{\text{CF}} + \hat{H}_{\text{CCF}}, \quad (1)$$

where \hat{H}_a denotes an ‘‘atomic’’ Hamiltonian that includes the isotropic interactions, i.e., interactions that are characteristic of the free-ion $4f^{11}$ electron configuration as well as the spherically symmetric crystal-field component B_0^0 defined later. In Eq. (1), \hat{H}_{CF} and \hat{H}_{CCF} represent the nonspherical components of the crystal-field interactions, and they consist of one-electron and correlated two-electron interaction operators, respectively.²⁶

The ‘‘atomic’’ Hamiltonian \hat{H}_a includes electrostatic (Coulomb) interactions between the $4f$ electrons (\hat{H}_{ee}), the spin-orbit interactions (\hat{H}_{so}) and the minor interactions \hat{H}_{ee2} , \hat{H}_{ee3} , \hat{H}_{soo} , and \hat{H}_{ci} . It can be written as

$$\begin{aligned} \hat{H}_a &= E_{\text{avg}} + \hat{H}_{ee} + \hat{H}_{so} + \hat{H}_{ee2} + \hat{H}_{ee3} + \hat{H}_{soo} + \hat{H}_{ci} \\ &= E_{\text{avg}} + \sum_k F^k \hat{f}_k + \zeta \hat{A}_{so} + \alpha \hat{L}(\hat{L}+1) + \beta \hat{G}(G_2) \\ &\quad + \gamma \hat{G}(R_7) + \sum_i T^i \hat{t}_i + \sum_j M^j \hat{m}_j + \sum_k P^k \hat{p}_k \end{aligned} \quad (2)$$

where $k=2,4,6$; $i=2,3,4,6,7,8$; and $j=0,2,4$.^{27,28} The E_{avg} parameter in Eq. (2) provides an equal baricenter shift for all $2^{2S+1}L_J$ multiplets and summarizes interactions that are independent of angular coordinates, such as the kinetic energy of the $4f$ electrons, the electrostatic interactions between $4f$

electrons and nucleus, the isotropic crystal-field parameter B_0^0 (Madelung constant²⁹), and the F^0 radial integrals from intraconfigurational and interconfigurational electrostatic interactions.

In rare-earth ions, \hat{H}_{ee} and \hat{H}_{so} are of comparable magnitude and typically represent about 80–90% of the “atomic” components in Eq. (1) (Refs. 22, 23, 27, and 30–32]. For this reason, most electronic energy-level calculations only consider \hat{H}_{ee} and \hat{H}_{so} in their “atomic” Hamiltonian, an approach usually referred to as *intermediate coupling*.³³ The quantitative prediction and analysis of excitation and relaxation processes, however, requires the precise knowledge of both the crystal-field energies and the oscillator strengths of the electronic transitions involved. For example, a 12-cm⁻¹ energy mismatch is sufficient to reverse the relative efficiency of energy-transfer upconversion and excited-state absorption processes from the $^4I_{11/2}$ state in Er³⁺-doped Cs₃Lu₂Br₉.¹⁵ A calculation able to predict such processes must therefore offer an energy uncertainty of less than 0.1%, making it necessary to also include minor atomic interactions in \hat{H}_a .^{27,28,34–38} The four most relevant minor atomic interactions included in Eq. (2) are discussed in the following.

\hat{H}_{ee} is an even-parity operator and couples states of the same L and S through electrostatic interactions within the $4f^{11}$ electron configuration. In analogy, states within this configuration can couple through weak electrostatic interactions with states of *different* electron configurations and the same parity. This two-body interconfigurational electrostatic interaction can be treated by second-order perturbation theory, and the radial part of \hat{H}_{ee2} is described by the parameters α , β , and γ .³⁴ Similarly, $|SL\rangle$ states of different $4f$ configurations can couple through weak three-body interconfigurational electrostatic interactions (\hat{H}_{ee3}) and be parametrized in terms of T^i ($i=2,3,4,6,7,8$).^{34,35} In contrast to \hat{H}_{ee} , which couples states of similar energies, the perturbing states in \hat{H}_{ee2} and \hat{H}_{ee3} are separated from the $4f$ ground configuration by some 100 000 cm⁻¹ and their contribution is therefore small relative to \hat{H}_{ee} . Nevertheless, they mix $|SL\rangle$ states and, collectively, contribute significantly to the respective energies.

The major part of the spin-orbit interactions is determined by \hat{H}_{so} , the (conventional) coupling of the spin magnetic moment and the orbital magnetic moment of a single $4f$ electron. Alternatively, the spin and orbital magnetic moments of *different* $4f$ electrons in the same configuration can couple and \hat{H}_{soo} describes the subsequent coupling of the resulting total net spin and net orbital magnetic moments.³⁶ The radial part (Marvin integrals) of this correlated two-body spin-orbit interaction is parametrized in terms of M^j ($j=0,2,4$), and \hat{H}_{soo} weakly affects $|SLJ\rangle$ energies in the same way \hat{H}_{so} does. As a result of electrostatic interactions between $|SL\rangle$ states of the $4f$ ground and $4f$ *excited* configurations, the net angular momentum of the individual $4f$ electrons is changed relative to its unperturbed value. This electrostatically correlated spin-orbit interaction (\hat{H}_{ci}) is parametrized in terms of P^k ($k=2,4,6$) (Refs. 37 and 38) and represents a small correction to the one-electron spin-orbit coupling constant ζ .

The \hat{H}_{CF} and \hat{H}_{CCF} operators in Eq. (1) represent the non-spherical components of the crystal-field interactions. The interaction of individual $4f$ electrons with the crystal-field potential is described by \hat{H}_{CF} , an operator that is commonly defined as

$$\hat{H}_{CF} = \sum_{k,q} B_q^k \hat{U}_q^k \quad (3)$$

for $4f$ and $5f$ ions.^{26,28,39} The \hat{U}_q^k are unit tensor operators that represent the angular dependence, and B_q^k are parameters that represent the radial part of the crystal-field interaction. Since the $4f$ wave functions are linear combinations of (odd-parity) spherical harmonics, the rank k is limited to $k=0\dots6$, and only even-parity ($k=0,2,4,6$) \hat{U}_q^k operators yield nonzero contributions to Eq. (3). The crystal-field symmetry limits the order q , and for the assumed C_{3v} site symmetry of Er³⁺ in Cs₃Lu₂Cl₉ only $q=0,3,6$ provide rotational invariance under the operations of the point group. \hat{H}_{CF} is therefore defined as

$$\begin{aligned} \hat{H}_{CF} = & B_0^2 \hat{U}_0^2 + B_0^4 \hat{U}_0^4 + B_3^4 (\hat{U}_3^4 - \hat{U}_{-3}^4) + B_0^6 \hat{U}_0^6 \\ & + B_3^6 (\hat{U}_3^6 - \hat{U}_{-3}^6) + B_6^6 (\hat{U}_6^6 + \hat{U}_{-6}^6). \end{aligned} \quad (4)$$

The spherically symmetric B_0^0 term has been omitted in Eq. (4) since it is already included in E_{avg} [Eq. (2)]. In addition to the interaction of individual $4f$ electrons with the crystal-field potential \hat{H}_{CF} , a smaller contribution from the simultaneous interaction of two $4f$ electrons and the crystal-field potential has to be considered.^{26,39–42} This correlated crystal-field interaction is described by

$$\hat{H}_{CCF} = \sum_{i,k,q} G_{iq}^k \hat{g}_{iq}^k, \quad (5)$$

where, in analogy to \hat{H}_{CF} , the rank $k=0\dots12$ and the order q is restricted by the crystal-field symmetry, i distinguishes different operators having the same k , \hat{g}_{iq}^k are orthogonal correlation crystal-field (CCF) operators, and G_{iq}^k are the respective parameters.^{26,40,43} Some of the $G_{iq}^k \hat{g}_{iq}^k$ terms are excluded from Eq. (5) because they are already accounted for in \hat{H}_a and \hat{H}_{CF} . Nevertheless, there remain 40 nonzero $G_{iq}^k \hat{g}_{iq}^k$ terms in Eq. (5). The inclusion of all of these CCF terms to the Hamiltonian is impractical due to the experimental limitations on the number of available crystal-field levels, and the selection of a relevant subset of CCF parameters is required. The crystal-field splitting of some $^{2S+1}L_J$ multiplets is known to be poorly characterized by the \hat{H}_{CF} operator.^{21,44,45} In particular, the crystal-field splitting of multiplets with $J=9/2$ or $J=11/2$ in $4f^3$ and $4f^{11}$ systems is consistently over or underestimated by \hat{H}_{CF} ,^{21,26,46,47} and targeting these states with appropriate CCF operators may provide a significant improvement in the characterization of the electronic energy-level structure. Li and Reid have shown that adding the fourth-rank CCF operator \hat{g}_{10A}^4 to the Hamiltonian greatly improves the calculated crystal-field energies of these multiplets for Nd³⁺ in Y₃Al₅O₁₂

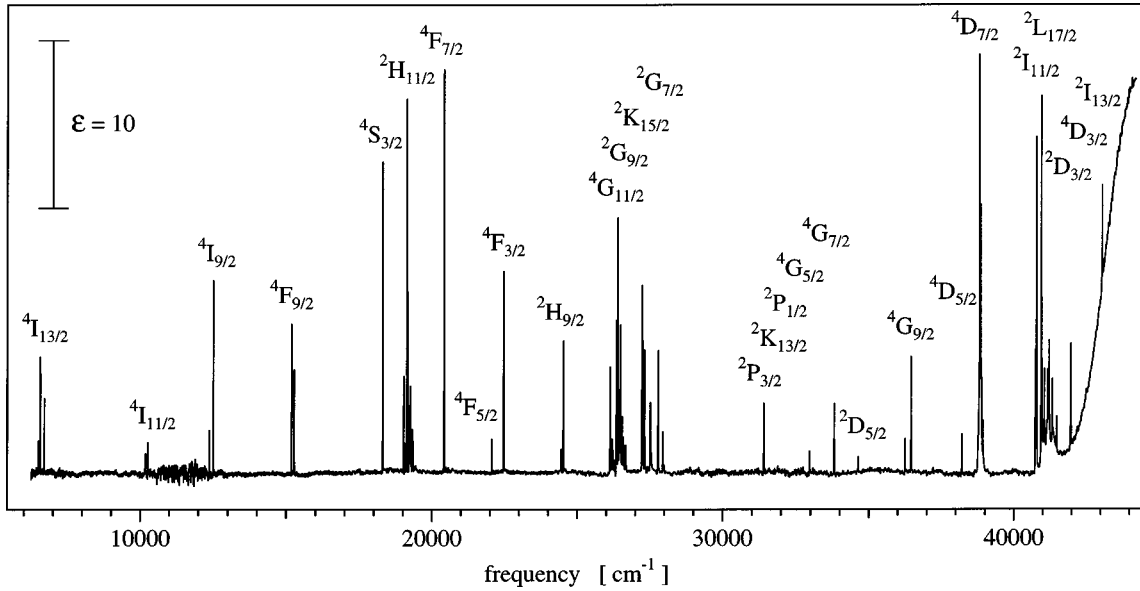


FIG. 1. π -polarized survey absorption spectrum of $\text{Cs}_3\text{Lu}_2\text{Cl}_9:1\% \text{Er}^{3+}$ at 10 K. The $^{25+1}L_J$ multiplets are labeled conventionally (Refs. 63 and 64) even in those very few cases in which the term does not represent the biggest contribution to the wave function in our calculation.

(YAG), LaCl_3 , LiYF_4 , LaF_3 , NdAlO_3 , $\text{Na}_3[\text{Nd}(\text{C}_4\text{H}_4\text{O}_5)_3 \cdot 2\text{NaClO}_4]_3(\text{NdODA})$.⁴³ For this reason we use their definition,

$$\hat{H}_{\text{CCF}} = \sum_{q=0,3} G_{10Aq}^4 \hat{g}_{10Aq}^4, \quad (6)$$

and, with the fixed ratio $G_{10A3}^4 = (B_3^4/B_0^4)G_{10A0}^4$, the CCF Hamiltonian used in the present calculation is given by

$$\hat{H}_{\text{CCF}} = G_{10A0}^4 \left(\hat{g}_{10A0}^4 + \frac{B_3^4}{B_0^4} \hat{g}_{10A3}^4 \right). \quad (7)$$

Equation (7) introduces only one additional fitting parameter to the Hamiltonian and has been successfully used in electronic energy-level calculations in a variety of Nd^{3+} - and Er^{3+} -doped crystals.^{16,22,23,31,32,43,48}

B. Intensities of crystal-field transitions

The intensity calculations performed in this study are based on the f - f intensity model described by Reid and Richardson.^{49,50} In their approach, electric-dipole transition line strengths are expressed as sums of irreducible unit tensor matrix elements (U_i^λ) over the crystal-field states (entirely defined within the $4f^n SLJM_J$ basis) and a set of parameters (A_{ip}^λ) that contain detailed and complete information about the interactions of the odd-parity crystal field and the electric-dipole radiation field with the $4f$ electrons of the system in the approximation of *one-photon-one-electron* f - f transition processes. The model is used in a phenomenological way: The parameters are determined by fitting calculated transition intensities to measured absorption intensities. The matrix elements for both electric-dipole (ED) and magnetic-dipole (MD) contributions to the transition intensities are calculated using the crystal-field eigenvectors from the energy-level calculations (see Sec. III A).

The *total* transition dipole strength D_{AB} for a transition between two crystal-field levels is thus given by

$$D_{AB} = D_{AB}^{\text{ED}} + D_{AB}^{\text{MD}} = \left| \sum_a \sum_b \sum_q \langle Aa | \hat{\mu}_q | Bb \rangle \right|^2 + \left| \sum_a \sum_b \sum_q \langle Aa | \hat{m}_q | Bb \rangle \right|^2, \quad (8)$$

where A and B denote the initial and final levels, respectively, and the summations are over all the degenerate components a and b of levels A and B , respectively, and over the spherical components ($q=0, \pm 1$) of the electric-dipole ($\hat{\mu}_q$) and the magnetic-dipole (\hat{m}_q) moment operators. In terms of the eigenvectors Ψ_{Aa} and Ψ_{Bb} obtained in the energy calculation in Sec. III the transition dipole strength D_{AB} for the q -polarized component of the electric-dipole and the magnetic-dipole operators can be expressed as^{49,50}

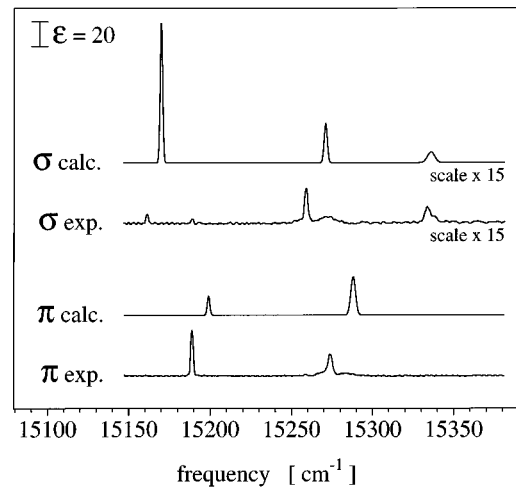


FIG. 2. Comparison of the calculated and experimental polarized ${}^4I_{15/2} \rightarrow {}^4F_{9/2}$ absorption spectra of $\text{Cs}_3\text{Lu}_2\text{Cl}_9:1\% \text{Er}^{3+}$ at 16 K. The wave functions from the CCF calculation and the parameters in Table III were used for the intensity calculation. The experimental line width of the individual transitions was used for the simulation of the spectra.

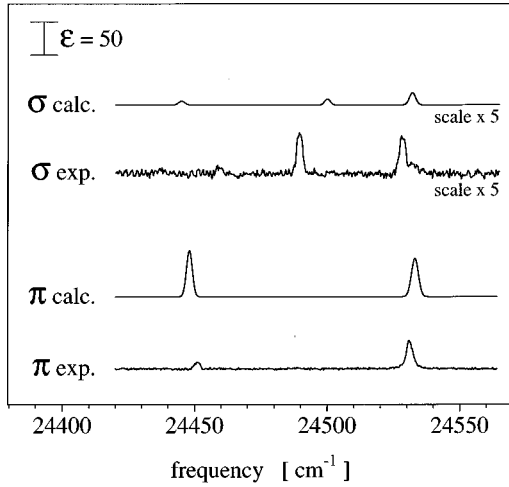


FIG. 3. As in Fig. 2, but for the ${}^4I_{15/2} \rightarrow {}^2H_{9/2}$ transition at 16 K.

$$\begin{aligned}
 D_{AB,q} = e^2 & \sum_{\lambda,t,p} A_{tp}^\lambda \sum_l \langle \lambda l, 1-q | tp \rangle \\
 & \times (-1)^q \sum_{a,b} \langle \Psi_{Aa} | \hat{U}_l^\lambda | \Psi_{Bb} \rangle^2 \\
 & + \left| \sum_{a,b} \langle \Psi_{Aa} | \hat{m}_q | \Psi_{Bb} \rangle \right|^2. \quad (9)
 \end{aligned}$$

In Eq. (9), A_{tp}^λ are the phenomenological intensity parameters containing structural and mechanistic details regarding interactions of the odd-parity crystal field and the electric-dipole radiation field with the $4f$ electrons of the system. They are defined by the rank (t), the order (p), and by $\lambda = t-1, t, t+1$. The $3j$ symbols restrict l to $p+q$. The polarization q is ± 1 and 0 for ED_σ , MD_π , and ED_π , MD_σ respectively.⁵¹ These operators represent the isotropic interactions ($t = \lambda \pm 1$), the anisotropic interaction operators ($t = \lambda$) were not included in the intensity analysis.⁵² No attempts were made to extract information about specific mechanistic contributions to electric-dipole intensity from the model. The chloride ligands are isotropic ligands treated in a simple static coupling model. In this description they are expected to be unresponsive to the incident radiation field. Being isotropic ligands, they are characterized by their net

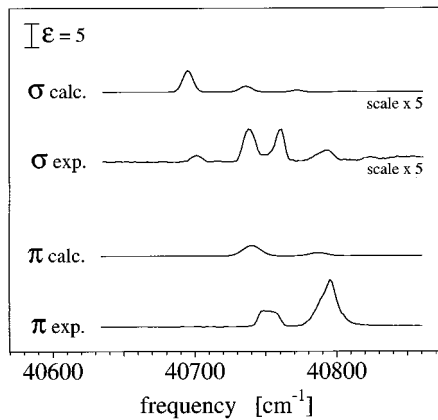


FIG. 4. As in Fig. 2, but for the ${}^4I_{15/2} \rightarrow {}^2I_{11/2}$ transition in the UV at 10 K.

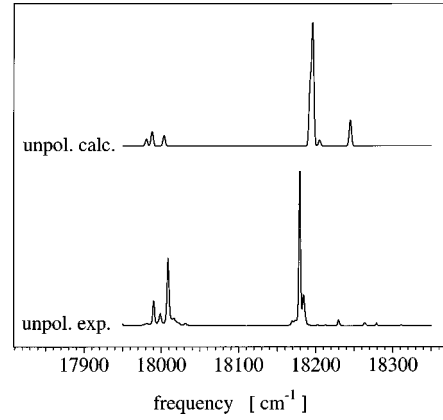


FIG. 5. Unpolarized calculated and experimental ${}^4S_{3/2} \rightarrow {}^4I_{15/2}$ luminescence spectra of $\text{Cs}_3\text{Lu}_2\text{Cl}_6:1\% \text{Er}^{3+}$ at 4.2 K. The total emission intensity is normalized to the calculated spectrum. The experimental linewidth of the individual transitions was used for the simulation of the spectrum.

charge, mean isotropic polarizability and vulnerability to charge polarization only from the lanthanide ion. For further information about possible mechanistic interpretations of the A_{tp}^λ parameters in the Reid-Richardson parametrization scheme, we refer the reader to Refs. 49 and 50.

Equation (9) provides the basis for performing a parametric analysis of empirical line-strength data in terms of A_{tp}^λ parameters. In our phenomenological approach, the set of A_{tp}^λ parameters only reflects the symmetry of the crystal field, and in the approximate C_{3v} site symmetry there are twelve parameters.^{49,50} In a first step, the A_{tp}^λ parameters are obtained from a fit of the line strengths [see Eq. (10), Sec. IV B] to experimental absorption intensities. Subsequently, the A_{tp}^λ parameters are used to predict line strengths of unobserved transitions and to simulate absorption and emission spectra.

IV. RESULTS

A. Spectroscopic results

A π -polarized survey absorption spectrum of $\text{Cs}_3\text{Lu}_2\text{Cl}_6:1\% \text{Er}^{3+}$ recorded at 10 K is shown in Fig. 1. Both the energies and relative intensities of the various f - f transitions are typical for Er^{3+} in a crystalline host, and the assignment to the respective ${}^{2S+1}L_J$ terms is straightforward from a comparison with the literature. A total of 26 ${}^{2S+1}L_J(4f^{11})$ multiplets in the NIR, the VIS, and the UV spectral regions were observed in absorption.

Figures 2, 3, and 4 show representative spectra of absorption at 10 and 16 K from the ${}^4I_{15/2}$ ground-state multiplet to the ${}^4F_{9/2}$ ($\sim 15\,250 \text{ cm}^{-1}$), ${}^2H_{9/2}$ ($\sim 24\,500 \text{ cm}^{-1}$), and ${}^2I_{11/2}$ ($\sim 40\,750 \text{ cm}^{-1}$) multiplets, respectively. The line widths in the absorption spectra are determined by the instrumental resolution, a limitation that is particularly obvious for the ${}^4I_{15/2} \rightarrow {}^2I_{11/2}$ transition in the UV. All the absorption transitions are almost perfectly polarized either σ or π . Figure 5 shows a representative of a luminescence spectrum of the ${}^4S_{3/2} \rightarrow {}^4I_{15/2}$ transition ($\sim 18\,300 \text{ cm}^{-1}$) at 4.2 K. From the combined information from the polarized absorption, upconversion luminescence, and excitation spectra, 114 crystal-field levels were identified, and are listed in Table I.

B. Computational results

The parameter set from $\text{Cs}_3\text{Lu}_2\text{Br}_9:1\% \text{Er}^{3+}$ (Ref. 23) was taken as the starting point for the energy calculations reported here. With an initial small set of experimental crystal-field levels mainly from the NIR and the VIS spectral region, the atomic part of the Hamiltonian [Eq. (2)] followed by the crystal-field part [Eq. (4)] were allowed to optimize separately. As the standard deviation improved, more experimental energy levels were included in an iterative process. In the final least-squares calculation, all the atomic, crystal-field, and CCF parameters [Eq. (1)] were allowed to vary simultaneously. The energies and parameter values from the final calculation, which included 111 experimental crystal-field levels, are reported in Tables I and II. A root-mean-square (rms) standard deviation of 17.98 cm^{-1} was obtained from the full model. A calculation excluding the CCF interactions gave a rms standard deviation of 22.75 cm^{-1} for the same experimental data set. A third calculation including only \hat{H}_{ee} , \hat{H}_{so} , and \hat{H}_{CF} , gave a rms standard deviation of 159.8 cm^{-1} , illustrating the importance of the various minor atomic and CCF interactions accounted for in the full model.

The empirical data set used for the intensity calculations consisted of 95 intensities of transitions from the ${}^4\text{I}_{15/2}(0)$ ground level to all crystal-field levels ranging from ${}^4\text{I}_{13/2}$ (6500 cm^{-1}) up to ${}^2\text{I}_{13/2}$ ($43\,450 \text{ cm}^{-1}$), derived from the 10- and 16-K absorption measurements. Assuming only electric-dipole and magnetic-dipole contributions to the observed intensities, the transition line strength of a crystal-field transition $A \rightarrow B$, $S_{AB,q}$, is given by

$$S_{AB,q} = D_{AB,q}^{\text{ED}} \chi_q^{\text{ED}} + D_{AB,q}^{\text{MD}} \chi_q^{\text{MD}} \quad (10)$$

with the transition dipole strengths $D_{AB,q}^{\text{ED}}$ and $D_{AB,q}^{\text{MD}}$, and the local-field correction factors χ_q^{ED} and χ_q^{MD} for the electric-dipole and magnetic-dipole components of the radiation field, respectively. The polarization q is ± 1 and 0 for ED_σ , MD_π and ED_π , MD_σ , respectively. All features in the spectra could be consistently interpreted on the basis of the electric-dipole transition mechanism for the intensity calculations predict the magnetic-dipole contributions to be weaker than the electric-dipole contributions by a factor of 10^3 to 10^6 . The line strengths S_{AB} , in squared Debye units (D^2), are calculated from the absorption spectra, which are represented in ϵ units ($1 \text{ mol}^{-1} \text{ cm}^{-1}$) versus wave numbers (cm^{-1}), using

$$S_{AB} = \frac{3 \cdot h \cdot \epsilon_0 \cdot c \cdot \ln(10)}{2 \pi^2 \cdot N_A \cdot \tilde{\nu} \cdot \chi^{\text{ED}}} \int \epsilon(\tilde{\nu}) d\tilde{\nu}, \quad (11)$$

where

$$\chi^{\text{ED}} = \frac{(n^2 + 2)^2}{9n} \quad (12)$$

is the local-field correction factor, $n \approx 1.8$ the index of refraction,⁵³ ϵ_0 is the vacuum permittivity in ($\text{C}^2 \text{ J}^{-1} \text{ m}^{-1}$) units, and N_A Avogadro's number. Note that $\tilde{\nu}$ denotes the mean transition frequency, derived from the integration over the entire line profile.

Since the chloride anions are isotropic ligands, the A_{tp}^λ parameters are zero for $\lambda = t$. Furthermore, in C_{3v} symmetry

the A_{tp}^λ parameters are real and restricted to the (λ, t, p) combinations $(2,1,0)$, $(2,3,0)$, $(2,3,\pm 3)$, $(4,3,0)$, $(4,3,\pm 3)$, $(4,5,0)$, $(4,5,\pm 3)$, $(6,5,0)$, $(6,5,\pm 3)$, $(6,7,0)$, $(6,7,\pm 3)$, and $(6,7,\pm 6)$.^{49,50} Each A_{tp}^λ parameter was given an initial value of 10^{-11} cm for the fitting procedure. They were first fitted to a small set of experimental intensities from the NIR and the VIS spectral range and were only allowed to optimize within subsets of the same λ . As the parameters became stable, the experimental data set was enlarged to include all the 95 individual intensities from the NIR up to the UV spectral range. In the late stage of the fitting procedure, all A_{tp}^λ parameters were allowed to simultaneously vary freely. The final A_{tp}^λ parameter values are collected in Table III. Table I compares experimental line strengths for absorption transitions from the ${}^4\text{I}_{15/2}(0)$ level with the respective line strengths S_{AB} calculated using the final A_{tp}^λ parameter set (Table III) and Eq. (10). Figures 2, 3, and 4 compare simulated and experimental absorption spectra for some selected transitions in different wavelength regions from the red to the UV spectral range. As an example of a luminescence transition, experimental and calculated spectra for the ${}^4\text{S}_{3/2} \rightarrow {}^4\text{I}_{15/2}$ transition are compared in Fig. 5.

V. DISCUSSION

A. Crystal-field splittings and irreducible representations

The $\text{Cs}_3\text{Lu}_2\text{Cl}_9$ crystal system belongs to the $R\bar{3}c$ space group⁵⁴ and Er^{3+} ions doped into $\text{Cs}_3\text{Lu}_2\text{Cl}_9$ substitute for Lu^{3+} ions. The $[\text{Lu}_2\text{Cl}_9]^{3-}$ dimeric building blocks of the lattice consist of two trigonally distorted, face-sharing $[\text{LuCl}_6]^{3-}$ octahedra. The hexagonal c axis of the crystal lattice coincides with the trigonal axis of the $[\text{Lu}_2\text{Cl}_9]^{3-}$ dimer. The $\text{Lu}^{3+} - \text{Cl}^-$ bond lengths are 2.685 \AA and 2.461 \AA for the bridging and terminal Cl^- , respectively, lowering the Lu^{3+} point symmetry from O_h to C_{3v} . In addition, there is a small twist of 1.02° of the three terminal relative to the three bridging Cl^- ions, resulting in an effective C_3 site symmetry for the Lu^{3+} ions. Since this distortion from C_{3v} to C_3 is small, the model calculations were carried out in the approximate C_{3v} point symmetry thus ignoring the small twist.

Because the Er^{3+} site lacks a center of inversion, electric-dipole-induced transitions are allowed and provide most of the intensity to the crystal-field transitions. In the C_{3v} double group, the selection rules for electric-dipole transitions are given by

	$E_{1/2}$	$E_{3/2}$
$E_{1/2}$	π, σ	σ
$E_{3/2}$	σ	π

where σ and π refer to the perpendicular and parallel orientation of the electric vector E of the electromagnetic field relative to the c axis the crystal lattice, respectively, and $E_{1/2}$ and $E_{3/2}$ denote the irreps of the C_{3v} double group.⁵⁵ They correspond to Γ_4 and $\Gamma_5 + \Gamma_6$, respectively, in Bethe notation. In contrast to an $E_{1/2}$ initial state, the polarization of crystal-field transitions is complementary for an $E_{3/2}$ initial state, i.e., $E_{3/2} \rightarrow E_{1/2}$ and $E_{3/2} \rightarrow E_{3/2}$ are purely σ and π polarized, respectively. The complementary polarization prop-

TABLE I. Experimental and calculated energy levels (in cm^{-1}) and line strengths S_{AB} (in 10^{-8}D^2) for $\text{Cs}_3\text{Lu}_2\text{Cl}_9:1\% \text{Er}^{3+}$. The parameter set used for the energy level and the intensity calculation is given in Tables II and III, respectively. Conventional multiplet labels are used even in those very few cases in which this is not the biggest contribution to the wave function in our calculation.^{63,64} The assignment to the irreps of the C_{3v} point group is determined experimentally or taken from the calculation for levels not observed. Energy levels marked by an asterisk are in a different calculated irrep ordering than observed experimentally. Experimental levels given in parentheses were excluded from the calculations.

Level	Multiplet	Irrep	Energy			Line strength			
			Expt.	Calc.	Δ	σ_{obs}	σ_{calc}	π_{obs}	π_{calc}
0	$4I_{15/2}$	$E_{3/2}$	0	-24.3	24.3				
1	$4I_{15/2}$	$E_{1/2}$	49	24.2	24.8				
2	$4I_{15/2}$	$E_{1/2}$	94	73.1	20.9				
3	$4I_{15/2}$	$E_{1/2}$	99	76.5	22.5				
4	$4I_{15/2}$	$E_{3/2}$	110	85.5	24.5				
5	$4I_{15/2}$	$E_{1/2}$	281	265.5	15.5				
6	$4I_{15/2}$	$E_{3/2}$	289	280.9	8.1				
7	$4I_{15/2}$	$E_{1/2}$	299	288.3	10.7				
8	$4I_{13/2}$	$E_{1/2}$	6508	6508.5	-0.5	1541	1569		
9	$4I_{13/2}$	$E_{1/2}$	6554	6559.8	-5.8	5789	1215		
10	$4I_{13/2}$	$E_{3/2}$	6572	6579.1	-7.1			3381	2240
11	$4I_{13/2}$	$E_{1/2}$	6582	6588.6	-6.6	371	646		
12	$4I_{13/2}$	$E_{1/2}$	6697	6721.2	-24.2		4190		
13	$4I_{13/2}$	$E_{3/2}$	6701	6721.2	-20.2			5742	8172
14	$4I_{13/2}$	$E_{1/2}$	6706	6722.1	-16.1		925		
15	$4I_{11/2}$	$E_{1/2}$	10 180	10 183.4	-3.4	106	106		
16	$4I_{11/2}$	$E_{3/2}$	10 208	10 215.7	-7.7			757	13 176
17	$4I_{11/2}$	$E_{1/2}$	10 216	10 227.1	-11.1		489		
18	$4I_{11/2}$	$E_{3/2}$	10 256	10 271.8	-15.8			1163	6932
19	$4I_{11/2}$	$E_{1/2}$	10 257	10 272.3	-15.3	217	976		
20	$4I_{11/2}$	$E_{1/2}$	10 265	10 274.7	-9.7		360		
21	$4I_{9/2}$	$E_{3/2}$	12 380	12 363.8	16.2			503	861
22	$4I_{9/2}$	$E_{1/2}$	12 409	12 381.4	27.6	66	208		
23	$4I_{9/2}$	$E_{1/2}$	12 454	12 449.6	4.4		50		
24	$4I_{9/2}$	$E_{1/2}$	12 509	12 496.1*	12.9	65	84*		
25	$4I_{9/2}$	$E_{3/2}$	12 513	12 496.0*	17.0				868*
26	$4F_{9/2}$	$E_{1/2}$	15 161	15 170.1	-9.1	36	527		
27	$4F_{9/2}$	$E_{3/2}$	15 189	15 199.3	-10.3			2466	982
28	$4F_{9/2}$	$E_{1/2}$	15 259	15 270.7	-11.7	206	247		
29	$4F_{9/2}$	$E_{3/2}$	15 274	15 288.4	-14.4			1891	3654
30	$4F_{9/2}$	$E_{1/2}$	15 334	15 336.2	-2.2	187	150		
31	$4S_{3/2}$	$E_{1/2}$	18 278	18 268.7	9.3	77	60		
32	$4S_{3/2}$	$E_{3/2}$	18 311	18 309.4	1.6			5567	8375
33	$2H_{11/2}$	$E_{1/2}$	19 020	19 048.8	-28.8	379	959		
34	$2H_{11/2}$	$E_{3/2}$	19 032	19 054.9	-22.9			698	998
35	$2H_{11/2}$	$E_{1/2}$	19 058	19 073.9	-15.9	1951	3679		
36	$2H_{11/2}$	$E_{3/2}$	19 142	19 183.0*	-41.0			2005	13 834*
37	$2H_{11/2}$	$E_{1/2}$	19 152	19 177.8*	-25.8		28 369*		
38	$2H_{11/2}$	$E_{1/2}$	19 175	19 218.3	-43.3	12 538	12 211		
39	$4F_{7/2}$	$E_{1/2}$	20 390	20 383.2	6.8	590	555		
40	$4F_{7/2}$	$E_{3/2}$	20 429	20 421.8	7.2			7556	2648
41	$4F_{7/2}$	$E_{1/2}$	20 459	20 445.5	13.5	1491	389		
42	$4F_{7/2}$	$E_{1/2}$	20 500	20 498.9	1.1	206	161		
43	$4F_{5/2}$	$E_{1/2}$	22 065	22 078.5	-13.5	309	459		
44	$4F_{5/2}$	$E_{3/2}$	22 073	22 084.0	-11.0			1031	931
45	$4F_{5/2}$	$E_{1/2}$	22 138	22 134.8	3.2	110	285		
46	$4F_{3/2}$	$E_{1/2}$	22 436	22 434.2	1.8	12	104		
47	$4F_{3/2}$	$E_{3/2}$	22 471	22 486.6	-15.6			4954	4912

TABLE I. (Continued)

Level	Multiplet	Irrep	Energy			Line strength			
			Expt.	Calc.	Δ	σ_{obs}	σ_{calc}	π_{obs}	π_{calc}
48	$^2\text{H}_{9/2}$	$E_{3/2}$	24 451	24 448.1*	2.9			641	4125*
49	$^2\text{H}_{9/2}$	$E_{1/2}$	24 459	24 445.1*	13.9	122	60*		
50	$^2\text{H}_{9/2}$	$E_{1/2}$	24 489	24 500.0	-11.0	516	72		
51	$^2\text{H}_{9/2}$	$E_{1/2}$	24 528	24 532.3	-4.3	559	189		
52	$^2\text{H}_{9/2}$	$E_{3/2}$	24 531	24 533.1	-2.1			2779	4085
53	$^4\text{G}_{11/2}$	$E_{1/2}$	26 129	26 121.2	7.8	776	1069		
54	$^4\text{G}_{11/2}$	$E_{3/2}$	26 142	26 131.5	10.5			2442	2577
55	$^4\text{G}_{11/2}$	$E_{1/2}$	26 205	26 205.5	-0.5	4527	3207		
56	$^4\text{G}_{11/2}$	$E_{3/2}$	26 358	26 358.8	-0.8			3500	13 285
57	$^4\text{G}_{11/2}$	$E_{1/2}$	26 365	26 361.7	3.3	6033	26 533		
58	$^4\text{G}_{11/2}$	$E_{1/2}$	26 411	26 410.8	0.2	25 216	22 642		
59	$^2\text{G}_{9/2}$	$E_{1/2}$	27 200	27 197.3	2.7	404	230		
60	$^2\text{G}_{9/2}$	$E_{3/2}$	27 236	27 236.7	-0.7			3918	21 391
61	$^2\text{G}_{9/2}$	$E_{1/2}$	27 262	27 241.7	20.3	1085	396		
62	$^2\text{G}_{9/2}$	$E_{3/2}$	27 274	27 279.5	-5.5			3179	11 870
63	$^2\text{G}_{9/2}$	$E_{1/2}$	(27 274)	27 279.8			291		
64	$^2\text{K}_{15/2}$	$E_{3/2}$	27 325	27 332.6	-7.6			2834	3533
65	$^2\text{K}_{15/2}$	$E_{1/2}$	27 457	27 471.5	-14.5	288	383		
66	$^2\text{K}_{15/2}$	$E_{1/2}$	27 505	27 528.7	-23.7	270	523		
67	$^2\text{K}_{15/2}$	$E_{3/2}$	27 527	27 552.3	-25.3			2024	701
68	$^2\text{K}_{15/2}$	$E_{1/2}$		27 607.0			77		
69	$^2\text{K}_{15/2}$	$E_{1/2}$		27 777.3			1		
70	$^2\text{K}_{15/2}$	$E_{3/2}$	27 796	27 789.4	6.6			2716	354
71	$^2\text{K}_{15/2}$	$E_{1/2}$		27 790.4			16		
72	$^2\text{G}_{7/2}$	$E_{1/2}$		27 882.5			131		
73	$^2\text{G}_{7/2}$	$E_{1/2}$		27 941.6			39		
74	$^2\text{G}_{7/2}$	$E_{3/2}$		27 948.1					350
75	$^2\text{G}_{7/2}$	$E_{1/2}$		27 961.7			4		
76	$^2\text{P}_{3/2}$	$E_{1/2}$	31 357	31 358.7	-1.7	10	4		
77	$^2\text{P}_{3/2}$	$E_{3/2}$	31 415	31 430.2	-15.2			1014	619
78	$^2\text{K}_{13/2}$	$E_{1/2}$	32 597	32 574.2	22.8	96	176		
79	$^2\text{K}_{13/2}$	$E_{1/2}$	32 729	32 712.5	16.5	247	5		
80	$^2\text{K}_{13/2}$	$E_{3/2}$	32 764	32 750.7	13.3			76	46
81	$^2\text{P}_{1/2}$	$E_{1/2}$		32 780.7			33		
82	$^2\text{K}_{13/2}$	$E_{1/2}$	32 920	32 894.1	25.9	10	2		
83	$^4\text{G}_{5/2}$	$E_{3/2}$	32 985	32 986.7*	-1.7			112	15*
84	$^2\text{K}_{13/2}$	$E_{1/2}$	33 025	32 981.8*	43.2	69	25*		
85	$^4\text{G}_{5/2}$	$E_{1/2}$	33 033	33 005.4	27.6	34	15		
86	$^2\text{K}_{13/2}$	$E_{3/2}$	33 100	33 066.6	33.4			49	33
87	$^2\text{K}_{13/2}$	$E_{1/2}$	33 109	33 070.2	38.8	29	41		
88	$^4\text{G}_{5/2}$	$E_{1/2}$	33 240	33 266.8	-26.8	20	2		
89	$^4\text{G}_{7/2}$	$E_{1/2}$	33 761	33 753.6	7.4	34	3		
90	$^4\text{G}_{7/2}$	$E_{1/2}$	33 820	33 836.8*	-16.8	14	32*		
91	$^4\text{G}_{7/2}$	$E_{3/2}$	33 829	33 810.3*	18.7			296	15*
92	$^4\text{G}_{7/2}$	$E_{1/2}$	33 971	33 963.8	7.2	38	98		
93	$^2\text{D}_{5/2}$	$E_{1/2}$	34 588	34 543.7	44.3	22	9		
94	$^2\text{D}_{5/2}$	$E_{1/2}$	34 640	34 660.2*	-20.2	30	98*		
95	$^2\text{D}_{5/2}$	$E_{3/2}$	34 642	34 650.3*	-8.3			81	89*
96	$^4\text{G}_{9/2}$	$E_{1/2}$	36 265	36 277.1	-12.1	9	12		
97	$^4\text{G}_{9/2}$	$E_{3/2}$	(36 270)	36 277.8					342
98	$^4\text{G}_{9/2}$	$E_{1/2}$	36 272	36 302.9	-30.9	13	7		
99	$^4\text{G}_{9/2}$	$E_{1/2}$	36 471	36 432.3	38.7	18	41		
100	$^4\text{G}_{9/2}$	$E_{3/2}$	36 480	36 484.7	-4.7			731	613

TABLE I. (Continued)

Level	Multiplet	Irrep	Energy			Line strength			
			Expt.	Calc.	Δ	σ_{obs}	σ_{calc}	π_{obs}	π_{calc}
101	$^4D_{5/2}$	$E_{1/2}$	38 177	38 188.7	-11.7	24	32		
102	$^4D_{5/2}$	$E_{3/2}$	38 234	38 230.5	3.5			197	206
103	$^4D_{5/2}$	$E_{1/2}$	38 241	38 243.7	-2.7	82	110		
104	$^4D_{7/2}$	$E_{1/2}$	38 682	38 681.4	0.6	111	2554		
105	$^4D_{7/2}$	$E_{1/2}$	38 708	38 723.1	-15.1	115	202		
106	$^4D_{7/2}$	$E_{3/2}$	38 846	38 849.7	-3.7			3065	1730
107	$^4D_{7/2}$	$E_{1/2}$		38 952.0			333		
108	$^2I_{11/2}$	$E_{1/2}$	40 700	40 694.6	5.4	29	97		
109	$^2I_{11/2}$	$E_{1/2}$	40 737	40 735.8	1.2	158	27		
110	$^2I_{11/2}$	$E_{3/2}$	40 748	40 739.9	8.1			705	416
111	$^2I_{11/2}$	$E_{1/2}$	40 759	40 772.0	-13.0		8		
112	$^2I_{11/2}$	$E_{3/2}$	40 791	40 786.8	4.2			1880	66
113	$^2I_{11/2}$	$E_{1/2}$	(40 802)	40 804.6			1		
114	$^2L_{17/2}$	$E_{1/2}$	40 945	40 961.3	-16.3	2643	404		
115	$^2L_{17/2}$	$E_{3/2}$		41 087.4					5727
116	$^2L_{17/2}$	$E_{1/2}$		41 168.3			93		
117	$^2L_{17/2}$	$E_{1/2}$		41 226.0			4		
118	$^2L_{17/2}$	$E_{3/2}$		41 272.4					6
119	$^2L_{17/2}$	$E_{1/2}$		41 311.6			7		
120	$^2L_{17/2}$	$E_{1/2}$		41 344.9			38		
121	$^2L_{17/2}$	$E_{3/2}$		41 371.2					294
122	$^2L_{17/2}$	$E_{1/2}$		41 386.4			1		
123	$^2D_{3/2}$	$E_{1/2}$		41 901.3			4		
124	$^2D_{3/2}$	$E_{3/2}$	41 988	41 936.8	51.2			405	481
125	$^4D_{3/2}$	$E_{3/2}$	42 515	42 512.6	2.4			68	1
126	$^4D_{3/2}$	$E_{1/2}$		42 558.9			1		
127	$^2I_{13/2}$	$E_{1/2}$	43 057	43 078.3	-21.3	116	121		
128	$^2I_{13/2}$	$E_{1/2}$	43 068	43 090.0	-22.0	137	133		
129	$^2I_{13/2}$	$E_{3/2}$	43 073	43 100.6	-27.6			357	174
130	$^2I_{13/2}$	$E_{1/2}$	43 305	43 286.5	18.5	474	190		
131	$^2I_{13/2}$	$E_{1/2}$	43 335	43 331.9	3.1	1046	1		
132	$^2I_{13/2}$	$E_{3/2}$	43 391	43 392.4	-1.4			101	59
133	$^2I_{13/2}$	$E_{1/2}$		43 439.9			8		

erties observed in the 10- and 16-K absorption spectra therefore clearly identify the lowest crystal-field level $^4I_{15/2}(0)$ as $E_{3/2}$. With this irrep for the ground level the excited levels can be assigned consistently in the low-temperature absorption spectra (see Table I). In analogy, low-temperature polarized upconversion luminescence spectra not shown here were used to determine the energies and irreps of the eight crystal-field levels of the $^4I_{15/2}$ ground-state multiplet. The ordering of the two lowest irreps of $^4I_{15/2}$ is reversed with respect to the ordering observed in the isostructural $\text{Cs}_3\text{Lu}_2\text{Br}_9:1\% \text{Er}^{3+}$, resulting in a complete change in the polarization properties of the crystal-field transitions.²³

B. Atomic interactions

In this first part of the discussion of the electronic energy-level structure we focus on the atomic interactions and neglect the details of the crystal-field splittings. The energies of the SLJ multiplets are largely determined by the atomic interactions, and $4f^{11}$ baricenter energies

$$\bar{E}^{SLJ} = (J + \frac{1}{2})^{-1} \sum_{i=1}^{J+1/2} g_i E_i^{SLJ}$$

(where the degeneracy $g_i = 2$ and i sums over all crystal-field levels) are used to assess the quality of the atomic Hamiltonian \hat{H}_a [Eq. (2)] and to identify multiplets that are particularly sensitive to the minor atomic interactions discussed in Sec. III. Equation (2) describes the experimental baricenter energies with a rms standard deviation of 9 cm^{-1} , with a maximum baricenter deviation of 29 cm^{-1} for the $^2H_{11/2}$ (see Tables I and IV). A simplified atomic Hamiltonian excluding the minor atomic interactions yields a rms standard deviation of 127 cm^{-1} , and the $^2D_{5/2}$ multiplet is off by as much as 428 cm^{-1} . An average error in the baricenter energy of 127 cm^{-1} is comparable to typical overall crystal-field splittings of the multiplets. The crystal-field parameters, which will be included in a subsequent step, are therefore not able to reproduce the experimental crystal-field splitting pattern for most of the multiplets and thus have very limited

TABLE II. Parameter values (in cm^{-1}) obtained from three least-squares fits of the model described in Secs. III A and IV B to the experimental energies of $\text{Cs}_3\text{Lu}_2\text{Cl}_9:1\% \text{Er}^{3+}$ (from Table I). The ratios $G_{10A0}^4 = -0.830G_{10A3}^4$, $M^2 = 0.56M^0$, $M^4 = 0.38M^0$, $P^4 = 0.75P^2$, and $P^6 = 0.5P^2$ were used. N is the number of experimental energy levels included in the fit and σ is the rms standard deviation (in cm^{-1}).

Parameter	CCF	No CCF	No CCF/no minor atomic
E_{avg}	35 375	35 379	35 431
F^2	97 940	97 968	98 444
F^4	69 850	69 877	73 379
F^6	49 850	49 906	57 529
ζ	2365.92	2365.96	2334.60
α	17.13	17.17	
β	-647	-645	
γ	1747	1739	
T^2	299	299	
T^3	44.9	48.7	
T^4	35.6	37.7	
T^6	-312	-313	
T^7	213	217	
T^8	352	352	
M^0	4.15	4.10	
P^2	539	536	
B_0^2	526	548	209
B_0^4	-1035	-951	-923
B_3^4	1247	1276	1109
B_0^6	-208	-130	255
B_3^6	-185	-157	-236
B_6^6	-200	-267	-552
G_{10A3}^4	-736		
N	111	111	111
σ	17.98	22.75	159.8

physical meaning (see Table II). They largely have to account for the inadequacies in the atomic part of the Hamiltonian. Note that even the sign of the B_0^6 parameter is reversed. We conclude that all the terms in Eq. (2) are essential for the parameter values to have any physical significance. Note in Table II that upon exclusion of \hat{H}_{ee2} , \hat{H}_{ee3} , \hat{H}_{soo} , and \hat{H}_{ci} , the F^k and ζ parameters try to compensate for those minor atomic interactions, and as a result the F^k and ζ parameter values become unphysical.

Collectively, the minor atomic interactions mainly affect baricenter energies throughout the VIS and UV spectral region. The multiplets most sensitive to the inclusion of these interactions are ${}^2\text{H}_{11/2}$ and ${}^4\text{F}_{7/2}$ in the VIS, and ${}^2\text{P}_{3/2}$, ${}^2\text{D}_{5/2}$, and ${}^2\text{I}_{11/2}$ in the UV. The effect is less pronounced but still significant for a variety of other spectroscopically relevant multiplets in the VIS such as ${}^4\text{F}_{9/2}$, ${}^4\text{S}_{3/2}$, ${}^4\text{F}_{5/2}$, ${}^4\text{F}_{3/2}$, and ${}^4\text{G}_{11/2}$. The multiplets of the ${}^4\text{I}$ manifold in the NIR are quite well characterized by the major atomic interactions and show only slight improvement when the minor atomic interactions are included. The trend of increasing importance of \hat{H}_{ee2} , \hat{H}_{ee3} , \hat{H}_{soo} , and \hat{H}_{ci} with increasing multiplet energy is expected since these interactions are treated on the basis of

TABLE III. A_{ip}^λ intensity parameters for $\text{Cs}_3\text{Lu}_2\text{Cl}_9:1\% \text{Er}^{3+}$ obtained from a least-squares fit of Eq. (10) to the experimental intensities given in Table I. A_{ip}^λ values are real and given in 10^{-11}cm . χ^{ED} and χ^{MD} are the local-field correction factors for electric-dipole and magnetic-dipole transitions, respectively, and were calculated (Sec. IV B) from Eq. (12) using $n=1.8$. N is the number of experimental intensities included in the fit and σ is the rms standard deviation (in 10^{-8}D^2).

Parameter	
A_{10}^2	-12.09
A_{30}^2	77.88
A_{33}^2	15.83
A_{30}^4	4.68
A_{33}^4	7.39
A_{50}^4	-7.89
A_{53}^4	-9.55
A_{50}^6	-29.58
A_{53}^6	-11.71
A_{70}^6	41.51
A_{73}^6	18.61
A_{76}^6	5.22
χ^{ED}	1.7
χ^{MD}	1.8
N	95
σ	4024

perturbation theory, and the energy differences to the perturbing electron configurations other than $[\text{Xe}]4f^{11}$ is smaller for higher-energy multiplets. ${}^2\text{H}_{11/2}$, the baricenter energy of which is off by 29cm^{-1} , is particularly difficult to describe even within our detailed model. Even with the subsequent inclusion of crystal-field terms (Sec. V C) its energy deviation from experiment is one of the highest in the entire calculation (see Tables I and IV), showing the limitations of this description. Inspection of Table IV shows that for ${}^2\text{H}_{11/2}$ as well as some other multiplets it is mainly the baricenter energy that is responsible for the discrepancy between calculated and experimental energies. The crystal-field splitting itself is reproduced accurately. We conclude that even after the inclusion of all the terms in Eq. (2) the atomic Hamiltonian still suffers some deficiencies leading to systematic deviations of all the components of a given multiplet and degrading the overall quality of the fit.

Both the major and minor atomic parameter values (Table II) are very similar to those reported for $\text{Cs}_2\text{NaErCl}_6$ (Ref. 21) and $\text{LaCl}_3:\text{Er}^{3+}$ (Ref. 16) which were investigated using a similar model. The covalency of the $\text{Er}^{3+}-X^-$ bond increases due to the increasing polarizability of coordinating ions along the series $X = \text{F}, \text{Cl}, \text{Br}, \text{I}$. This causes (i) a decrease in the electron-electron repulsion and thus a decrease in the respective F^k parameters, and (ii) a decrease in the effective orbital angular momentum and thus a decrease in the spin-orbit coupling parameter ζ . These trends are confirmed by the parameter values obtained from detailed crystal-field studies of Er^{3+} -doped LaF_3 ,²⁷ $\text{Cs}_2\text{NaErCl}_6$,²¹ LaCl_3 ,¹⁶ and $\text{Cs}_3\text{Lu}_2\text{Br}_9$,²³ and also the parameter values of the present $\text{Cs}_3\text{Lu}_2\text{Cl}_9:1\% \text{Er}^{3+}$ fit well in this picture.

TABLE IV. Comparison of experimental and calculated baricenter energies and crystal-field splittings (in cm^{-1}) for the lowest four $J=9/2$ or $J=11/2$ multiplets in $\text{Cs}_3\text{Lu}_2\text{Cl}_9:1\% \text{Er}^{3+}$. The crystal-field splittings are reported relative to the respective baricenter energies for the three calculations using the parameter sets presented in Table II. The level numbering is the same as in Table I. Energy levels marked by an asterisk are in a different calculated irrep ordering than observed experimentally.

Multiplet	Level	Irrep	Expt.	Splitting from baricenter			
				Expt.	CCF	No CCF	No CCF/no minor atomic
$^4\text{I}_{11/2}$	Baricenter			10 230	10 241	10 241	10 210
	15	$E_{1/2}$	10 180	-50	-57	-69	-58
	16	$E_{3/2}$	10 208	-22	-25	-33	-32
	17	$E_{1/2}$	10 216	-14	-14	-25	-30
	18	$E_{3/2}$	10 256	26	31	44*	35
	19	$E_{1/2}$	10 257	27	31	39*	46*
$^4\text{I}_{9/2}$	20	$E_{1/2}$	10 265	35	34	46	39*
	Baricenter			12 453	12 437	12 439	12 438
	21	$E_{3/2}$	12 380	-73	-74	-93	-125
	22	$E_{1/2}$	12 409	-44	-56	-74	-64
	23	$E_{1/2}$	12 454	1	12	29	0
$^4\text{F}_{9/2}$	24	$E_{1/2}$	12 509	56	59*	73*	124*
	25	$E_{3/2}$	12 513	60	59*	65*	64*
	Baricenter			15 243	15 253	15 254	15 144
	26	$E_{1/2}$	15 161	-82	-83	-90	-77
	27	$E_{3/2}$	15 189	-54	-54	-60	-52
	28	$E_{1/2}$	15 259	16	18	18	12
$^2\text{H}_{11/2}$	29	$E_{3/2}$	15 274	31	35	43	29
	30	$E_{1/2}$	15 334	91	83	89	88
	Baricenter			19 097	19 126	19 122	19 396
	33	$E_{1/2}$	19 020	-77	-77	-50	-72
	34	$E_{3/2}$	19 032	-65	-71	-41	-37
	35	$E_{1/2}$	19 058	-39	-52	-26	-19
	36	$E_{3/2}$	19 142	45	57*	35*	43*
	37	$E_{1/2}$	19 152	55	52*	25*	26*
	38	$E_{1/2}$	19 175	78	92	56	61

C. Crystal-field interactions

The following discussion is based on calculations using the full atomic Hamiltonian [Eq. (2)]. As shown in Table II, the rms standard deviation improves from 22.75 to 17.98 cm^{-1} when the two-particle CCF operator \hat{H}_{CCF} [Eq. (7)] is used in addition to the one-particle crystal-field operator \hat{H}_{CF} [Eq. (4)]. Since the rms standard deviation is an overall measure of the quality of the calculation, it does not adequately reflect the effect of \hat{H}_{CCF} on individual, particularly sensitive multiplets. Remember the definition of \hat{H}_{CCF} in Eq. (6) intentionally targets multiplets that are unsatisfactorily described by Eq. (4). The \hat{g}_{10Aq}^4 operators ($q=0,3$) have large matrix elements for the problematic multiplets with $J=9/2$ or $J=11/2$ and are known to greatly improve the quality of the fit in those regions.^{22,23,31,32,43,48} The significant improvement of the predicted crystal-field splittings upon inclusion of CCF interactions in our system is shown in detail in Table IV for the $^4\text{I}_{11/2}$, $^4\text{I}_{9/2}$, $^4\text{F}_{9/2}$, and $^2\text{H}_{11/2}$ multiplets. The inclusion of the CCF operators \hat{g}_{10A0}^4 and \hat{g}_{10A3}^4 not only yields a very good quantitative description of the crystal-field splittings but also corrects the wrong irrep ordering in some cases (see Table IV). As expected, the inclusion of

CCF interactions have only little effect on the baricenter energies and on the atomic parameters (see Table II). On the other hand, there are significant changes in the B_q^k parameters. It was found in the $\text{LaCl}_3:\text{Er}^{3+}$ study¹⁶ that the inclusion of CCF terms in the Hamiltonian did not significantly improve the energy fit. This is in contrast to our results where the one CCF parameter improved the fit from a rms standard deviation of 22.75 to 17.98 cm^{-1} . This indicates that the CCF term in the present work tries to compensate for deficiencies of the model and thus acquires contributions that are not directly related to CCF interactions.

As expected from the similar crystal-field potential for Er^{3+} in $\text{Cs}_3\text{Lu}_2\text{Cl}_9$ and $\text{Cs}_3\text{Lu}_2\text{Br}_9$, the relative magnitudes of the crystal-field parameters B_q^k are comparable.²³ In particular, the ratio of the rank four crystal-field parameters (B_0^4/B_3^4), which defines the ratio of the G_{10A0}^4 and G_{10A3}^4 CCF parameters [Eq. (7)] only slightly changes from -0.830 for $\text{Cs}_3\text{Lu}_2\text{Cl}_9$ to -0.778 for $\text{Cs}_3\text{Lu}_2\text{Br}_9$. The CCF parameters G_{10A0}^4 and G_{10A3}^4 are related by the same ratio as B_0^4 and B_3^4 [see Eq. (7)]. The crystal-field parameters only represent the radial part of the Hamiltonian and have to be weighted with the respective angular part for direct comparison. For a

given lanthanide ion and point symmetry, however, the angular matrix elements are identical for the $X=\text{Cl}$ and $X=\text{Br}$ systems and the changes in the B_q^k parameter values reflect the changes in the respective radial part. The decrease in the B_q^k parameter values from $X=\text{Cl}$ to $X=\text{Br}$ therefore can be correlated with a decrease in the crystal-field strength at the Er^{3+} site, which is a result of the lengthening of the $\text{Er}^{3+}-X^-$ bonds by 4.6% from $X=\text{Cl}$ to $X=\text{Br}$. The same argument also applies for the quantitative comparison of the various atomic parameters (Sec. V B).

D. Transition intensities

Table I lists calculated and experimental dipole strengths in both polarizations for the absorption transitions from the lowest crystal-field level ${}^4I_{15/2}(0)$ of the ground-state multiplet. The absorption transitions to ${}^4F_{9/2}$, ${}^2H_{11/2}$, and ${}^2I_{11/2}$ (Figs. 2–4) and the ${}^4S_{3/2}\rightarrow{}^4I_{15/2}$ luminescence transition (Fig. 5) are representative for the quality of the intensity fit. The comparison of the calculated and experimental spectra shows an overall fair agreement of intensities. The calculation overestimates the total intensity for transitions in absorption, this being particularly evident for transitions in π polarization. Furthermore, the relative intensity distribution between the crystal-field levels of a particular SLJ multiplet is not well reproduced. For the ${}^4I_{15/2}(0)\rightarrow{}^4I_{13/2}$ transitions the calculated electric-dipole intensities are similar to the observed ones. We therefore conclude that any magnetic-dipole contributions to these transitions are of minor importance, despite the fact that they have $\Delta J = \pm 1$.⁵⁶

Comparing our results with those of similar studies in the literature, we find similar quality of energy and intensity reproduction in Refs. 51,57–60. However, a recent study of $f-f$ transitions in Er^{3+} -doped LaCl_3 (Ref. 16) has shown a significantly better agreement even though the quality of the data was comparable to the present study. A total of 21 parameters were fit to 73 energies, resulting in a rms standard deviation of 9.0 cm^{-1} , compared to the 17.98 cm^{-1} found in the present study using 111 energies and 23 parameters. Obviously, better wave functions were obtained in the $\text{LaCl}_3:1\%\text{ Er}^{3+}$ case with the result of an almost perfect reproduction of absolute and relative intensities. The point symmetry of La^{3+} in the LaCl_3 is *exactly* C_{3h} , whereas it is *approximately* C_{3v} for Lu^{3+} in the title compound $\text{Cs}_3\text{Lu}_2\text{Cl}_9$. We believe that this is the main reason for the above-mentioned differences. The twist of 1.02° about the C_3 axis of the terminal with respect to the bridging chloride

ions, which removes the vertical mirror planes for C_{3v} , apparently has a much bigger effect than expected. The use of the actual C_3 point group would have changed the six crystal-field parameters from pure real to complex and would have increased the number of intensity parameters from 12 pure real (C_{3v}) to 18 complex (C_3).^{61,62} In view of the number of parameters, a computational analysis using the exact C_3 point symmetry would not be possible with the present data set.

VI. CONCLUSIONS

The description of a high-quality data set on the basis of an effective Hamiltonian, including all the relevant terms discussed so far in the literature, provides a good reproduction of the crystal-field energies. With a rms standard deviation of 17.98 cm^{-1} in the energy calculation we achieved our goal of reproducing the energies with an accuracy of $10\text{--}20\text{ cm}^{-1}$.

A more important feature of the model is its ability to predict individual crystal-field transition intensities since they, to a large extent, determine possible excitation schemes for upconversion and provide the basis for identification of transitions with a large cross section for stimulated emission. However, the crystal-field transition intensities calculated here show only fair agreement with experiment. Compared to the energy calculation, the intensity calculation is more sensitive to deficiencies in the model wave functions. A large part of these deficiencies originates from the approximate C_{3v} point symmetry of the Hamiltonian for the actual C_3 point symmetry of Er^{3+} in $\text{Cs}_3\text{Lu}_2\text{Cl}_9$. We deem important to perform both energy and intensity calculations in the actual point symmetry, although a deviation from a higher symmetry may appear minute, as in our case. Only then may the model reveal its full ability to predict potential upconversion laser schemes.

ACKNOWLEDGMENTS

We thank G. Frei, N. Furer, and K. Krämer (Universität Bern, Switzerland) for their assistance in the sample preparation, N. J. Cockroft (formerly with the Los Alamos National Laboratory, Los Alamos, NM) for supporting this collaboration, and F. S. Richardson (University of Virginia, Charlottesville, VA) and M. F. Reid (University of Canterbury, New Zealand) for providing the computer programs. This work was supported in part by the Swiss National Science Foundation.

*Author to whom correspondence should be addressed.

¹F. E. Auzel, Proc. IEEE **61**, 758 (1973).

²J. C. Wright, in *Topics in Applied Physics: Radiationless Processes in Molecules and Condensed Phases*, edited by F. K. Fong (Springer, Berlin, 1976).

³*Modern Problems in Condensed Matter Sciences: Spectroscopy of Solids Containing Rare Earth Ions*, edited by A. A. Kaplyanskii and R. M. Macfarlane (North-Holland, Amsterdam, 1987).

⁴T. J. Whitley, C. A. Millar, R. Wyatt, M. C. Brierley, and D. Szebesta, Electron. Lett. **27**, 1785 (1991).

⁵M. Takahashi, R. Kanno, and Y. Kawamoto, Mater. Res. Bull. **28**, 557 (1993).

⁶L. F. Johnson and H. J. Guggenheim, Appl. Phys. Lett. **19**, 44 (1971).

⁷R. A. McFarlane, J. Opt. Soc. Am. B **11**, 871 (1994).

⁸A. J. Silversmith, W. Lenth, and R. M. MacFarlane, Appl. Phys. Lett. **51**, 1977 (1987).

⁹B. M. Antipenko, S. P. Voronin, and T. A. Privalova, Sov. Phys. Tech. Phys. **32**, 208 (1987).

¹⁰W. Lenth, A. J. Silversmith, and R. M. MacFarlane, in *Advances in Laser Science—III: Proceedings of the International Laser Science Conference*, edited by W. Lenth, A. J. Silversmith, and R. M. MacFarlane, AIP Conf. Proc. No. 172 (AIP, New York, 1988), p. 8.

- ¹¹F. Tong, W. P. Risk, R. M. MacFarlane, and W. Lenth, *Electron. Lett.* **25**, 1389 (1989).
- ¹²T. Hebert, R. Wannemacher, W. Lenth, and R. M. MacFarlane, *Appl. Phys. Lett.* **57**, 1727 (1990).
- ¹³R. M. MacFarlane, M. Robinson, and S. A. Pollack, *Proc. SPIE* **1223**, 294 (1990).
- ¹⁴R. Brede, E. Heumann, J. Koetke, T. Danger, G. Huber, and B. Chai, *Appl. Phys. Lett.* **63**, 2030 (1993).
- ¹⁵M. P. Hehlen, G. Frei, and H. U. Güdel, *Phys. Rev. B* **50**, 16 264 (1994).
- ¹⁶K. W. Krämer, H. U. Güdel, and R. N. Schwartz, *Phys. Rev. B* **56**, 13 830 (1997).
- ¹⁷B. R. Judd, *Phys. Rev.* **127**, 750 (1962).
- ¹⁸G. S. Ofelt, *J. Chem. Phys.* **37**, 511 (1962).
- ¹⁹R. P. Leavitt and C. A. Morrison, *J. Chem. Phys.* **73**, 749 (1980).
- ²⁰R. A. McFarlane, *OSA Proc. Adv. Solid State Lasers* **13**, 275 (1992).
- ²¹F. S. Richardson, M. F. Reid, J. J. Dallara, and R. D. Smith, *J. Chem. Phys.* **83**, 3813 (1985).
- ²²J. R. Quagliano, N. J. Cockroft, K. E. Gunde, and F. S. Richardson, *J. Chem. Phys.* **105**, 9812 (1996).
- ²³M. P. Hehlen, H. U. Güdel, and J. R. Quagliano, *J. Chem. Phys.* **101**, 10 303 (1994).
- ²⁴R. Blachnik and D. Selle, *Z. Anorg. Allg. Chem.* **454**, 90 (1979).
- ²⁵G. Meyer, *Synthesis of Lanthanide and Actinide Compounds* (Kluwer Academic, Dordrecht, 1991).
- ²⁶M. F. Reid, *J. Chem. Phys.* **87**, 2875 (1987).
- ²⁷W. T. Carnall, G. L. Goodman, K. Rajnak, and R. S. Rana, *J. Chem. Phys.* **90**, 3443 (1989).
- ²⁸C. A. Morrison, *Angular Momentum Theory Applied to Interactions in Solids* (Springer, Berlin, 1988).
- ²⁹H. L. Schlafer, G. Gliemann, *Basic Principles of Ligand Field Theory* (Wiley-Interscience, London, 1969).
- ³⁰J. B. Gruber, M. E. Hills, T. H. Allik, C. K. Jayasankar, J. R. Quagliano, and F. S. Richardson, *Phys. Rev. B* **41**, 7999 (1990).
- ³¹J. R. Quagliano, F. S. Richardson, and M. F. Reid, *J. Alloys Compd.* **180**, 131 (1992).
- ³²J. B. Gruber, J. R. Quagliano, M. F. Reid, F. S. Richardson, M. E. Hills, M. D. Seltzer, S. B. Stevens, C. A. Morrison, and T. H. Allik, *Phys. Rev. B* **48**, 15 561 (1993).
- ³³B. R. Judd, *Proc. Phys. Soc. London, Sect. A* **69**, 157 (1956).
- ³⁴K. Rajnak and B. G. Wybourne, *Phys. Rev.* **132**, 280 (1963).
- ³⁵B. R. Judd, *Phys. Rev.* **141**, 1 (1966).
- ³⁶H. Horie, *Prog. Theor. Phys.* **10**, 296 (1953).
- ³⁷B. R. Judd, H. Crosswhite, and H. M. Crosswhite, *Phys. Rev.* **169**, 130 (1968).
- ³⁸W. T. Carnall, H. Crosswhite, and H. M. Crosswhite, *Energy Level Structure and Transition Probabilities in the Spectra of Trivalent Lanthanides in LaF₃* (Argonne National Laboratory, 1977).
- ³⁹D. J. Newman and B. Ng, *Rep. Prog. Phys.* **52**, 699 (1989).
- ⁴⁰B. R. Judd, *J. Chem. Phys.* **66**, 3163 (1977).
- ⁴¹B. R. Judd, *Phys. Rev. Lett.* **39**, 242 (1977).
- ⁴²H. Crosswhite and D. J. Newman, *J. Chem. Phys.* **81**, 4959 (1984).
- ⁴³C. L. Li and M. F. Reid, *Phys. Rev. B* **42**, 1903 (1990).
- ⁴⁴B. G. Wybourne, *Spectroscopic Properties of Rare Earth* (Interscience, New York, 1965).
- ⁴⁵C. A. Morrison and R. P. Leavitt, *J. Chem. Phys.* **71**, 2366 (1979).
- ⁴⁶C. A. Morrison, P. R. Fields, and W. T. Carnall, *Phys. Rev. B* **2**, 1526 (1970).
- ⁴⁷J. R. Quagliano, Dissertation, University of Virginia, Charlottesville, VA, 1993.
- ⁴⁸J. B. Gruber, J. R. Quagliano, M. F. Reid, F. S. Richardson, M. E. Hills, M. D. Seltzer, S. B. Stevens, C. A. Morrison, and T. H. Allik, *Phys. Rev. B* **48**, 15 561 (1993).
- ⁴⁹M. F. Reid and F. S. Richardson, *J. Chem. Phys.* **79**, 5735 (1983).
- ⁵⁰M. F. Reid and F. S. Richardson, *J. Phys. Chem.* **88**, 3579 (1984).
- ⁵¹P. S. May, C. K. Jayasankar, and F. S. Richardson, *Chem. Phys.* **138**, 139 (1989).
- ⁵²G. W. Burdick, C. K. Jayasankar, F. S. Richardson, and M. F. Reid, *Phys. Rev. B* **50**, 16 309 (1994).
- ⁵³G. F. Imbusch, in *Luminescence Spectroscopy*, edited by M. D. Lumb (Academic, London, 1978), p. 27.
- ⁵⁴G. Meyer, *Prog. Solid State Chem.* **14**, 141 (1982).
- ⁵⁵G. F. Koster, J. O. Dimmock, R. G. Wheeler, and H. Statz, *Properties of the Thirty-Two Point Groups* (MIT Press, Cambridge, 1963).
- ⁵⁶M. Tinkham, *Group Theory and Quantum Mechanics* (McGraw-Hill, New York, 1964).
- ⁵⁷P. S. May, M. F. Reid, and F. S. Richardson, *Mol. Phys.* **61**, 1471 (1987).
- ⁵⁸M. T. Berry, C. Schwieters, and F. S. Richardson, *Chem. Phys.* **122**, 105 (1988).
- ⁵⁹D. M. Moran and F. S. Richardson, *Phys. Rev. B* **42**, 3331 (1990).
- ⁶⁰J. R. Quagliano, G. W. Burdick, D. P. Glover-Fischer, and F. S. Richardson, *Chem. Phys.* **201**, 321 (1995).
- ⁶¹C. A. Morrison and R. P. Leavitt, in *Handbook on the Physics and Chemistry of Rare Earths*, edited by K. A. Gschneidner, Jr. and L. Eyring (North-Holland, Amsterdam, 1982), Vol. 5.
- ⁶²J. J. Dallara, M. F. Reid, and F. S. Richardson, *J. Phys. Chem.* **88**, 3587 (1984).
- ⁶³G. H. Dieke, *Spectra and Energy Levels of Rare Earth Ions in Crystals*, edited by H. M. Crosswhite and H. Crosswhite (Interscience, New York, 1968).
- ⁶⁴S. Hüfner, *Optical Spectra of Transparent Rare Earth Compounds* (Academic, New York, 1978).